Computational Materials Science 79 (2013) 888–895

Contents lists available at ScienceDirect

Computational Materials Science

journal homepage: www.elsevier.com/locate/commatsci

Tight-binding studies of bulk properties and hydrogen vacancies in KBH_4

A. Shabaev [a], Khang Hoang [a,b], D.A. Papaconstantopoulos [a,*], M.J. Mehl [c], N. Kioussis [d]

[a] Computational Materials Science Center, George Mason University, Fairfax, VA 22030, USA
[b] Center for Computationally Assisted Science and Technology, North Dakota State University, Fargo, ND 58108, USA
[c] Center for Computational Materials Science, Naval Research Laboratory, Washington, DC 20375, USA
[d] Department of Physics, California State University, Northridge, CA 91330, USA

ARTICLE INFO

Article history:
Received 5 December 2012
Received in revised form 24 June 2013
Accepted 28 June 2013
Available online 19 August 2013

Keywords:
Tight binding
First principles
Hydrogen storage
Potassium borohydride
Hydrogen vacancies

ABSTRACT

We present computational studies of the bulk properties and hydrogen vacancies in KBH_4 using tight-binding (TB) calculations. The NRL-TB method was used to construct a TB Hamiltonian by fitting the density-functional theory (DFT) data for the electronic energies for the tetragonal and cubic phases of KBH_4 as a function of volume. Our approach allows for computationally efficient calculations of phonon frequencies and elastic constants, mean-square displacements, and formation energies of hydrogen vacancies using the static and molecular dynamics modules of the NRL-TB code. We find that the results for the bulk properties and hydrogen vacancies given by TB calculations are comparable to those given by DFT calculations.

1. Introduction

In the search for hydrogen storage materials, alkali borohydrides (MBH_4; M = Li, Na, K) are especially attractive because of the light weight and high number of hydrogen atoms per metal atom [1]. These materials, however, have high thermodynamic stability and exhibit limitations in hydrogen kinetics and/or reversibility, making them not very suitable for practical applications [2]. Computational studies of the structural, electronic, elastic, vibrational, and dynamic properties and the energetics of native defects are therefore needed in order to better understand the fundamental properties of these complex hydrides and their hydrogen kinetics [3–9].

In this paper we focus on a tight-binding parametrization of KBH_4 using the Naval Research Laboratory tight-binding (NRL-TB) scheme [10,11]. In Section 2 we give the basic equations used in the NRL-TB method and discuss details of the procedure we followed to fit to a database of density-functional theory (DFT) results obtained with a pseudopotential code. Previously we had used linearized augmented plane wave (LAPW) results to derive a tight-binding Hamiltonian for palladium (Pd) and palladium–hydrogen systems (PdH_x) [12,13]. In these works, we showed that the NRL-TB scheme works well for a transition-metal-based hydride system, reproducing the LAPW total energies and band structures and extending to molecular dynamics (MD) simulations of large systems going beyond the standard capabilities of DFT.

A tight-binding formulation of a borohydride such as KBH_4 presents a challenge because it is a light and soft material with energetic differences as a function of volume that are very small. This requires a substantially lower target for root mean square (rms) fitting errors than those that were adequate for PdH_x. KBH_4 is known to have a low temperature (LT) tetragonal phase which transforms into a high temperature (HT) partially filled face-centered cubic (fcc) phase at 65–70 K [14]. We performed DFT calculations as a function of volume for both the tetragonal and cubic phases and used them as an input to derive our TB parameters. Although the NRL-TB scheme can be applied with a non-orthogonal basis, the results presented in this paper are using an orthogonal basis. We chose the orthogonal Hamiltonian in order to reduce the number of TB parameters and because we found that in this case non-orthogonality did not give us any significant improvement of the fit. Our TB matrix contains the K 4*s* orbital, the B 2*p* orbitals, and the H 1*s* orbital, hence we diagonalize an 8×8 matrix per formula unit which makes the calculation very fast despite the fact that we are using close to 1000 atoms in our MD simulations. Our TB results reproduce the total energies of both the LT and HT phases very well as a function of volume, and produce an excellent agreement with independent (not included in the fit) results of the phonon frequencies. Also our study of hydrogen vacancies gives a good agreement with separate DFT calculations. In general our DFT results used in the TB fitting are consistent with those found by other groups [14–20].

* Corresponding author. Tel.: +1 703 993 3624; fax: +1 703 993 9300.
E-mail address: dpapacon@gmu.edu (D.A. Papaconstantopoulos).

0927-0256/$ - see front matter © 2013 Elsevier B.V. All rights reserved.
http://dx.doi.org/10.1016/j.commatsci.2013.06.055

This paper is organized as follows: In Section 2 we describe the NRL-TB method. In Section 3 we present the TB parameters and the results of our calculations for electronic structure, elastic constants, vibrational spectra, and mean-squared displacement. In Section 4 we discuss the formation energies for hydrogen vacancies and compare the results of our calculations using DFT and TB methods. Finally, we summarize our work in Section 5.

2. Methods

The total-energy calculations were performed using the generalized-gradient approximation [21] and the projector-augmented wave (PAW) [22,23] method as implemented in the Vienna Ab-Initio Simulation Package (VASP) code [24–27]. The configurations K $3p^6 4s^1$, B $2p^2 3s^1$, and H $1s$ were treated as valence electrons. For the tetragonal (LT) and cubic (HT) bulk phases, the calculations were performed using $7 \times 7 \times 5$ and $9 \times 9 \times 9$ Monkhorst–Pack **k**-point meshes [28], respectively. The plane-wave basis-set cutoff was set to 400 eV and convergence with respect to self-consistent iterations was assumed when the total energy difference between cycles was less than 10^{-4} eV and the residual forces were less than 0.01 eV/Å.

We carried out VASP calculations for both the tetragonal and cubic phases in a wide range of lattice constants (and, for the tetragonal phase, c/a ratios). The total energy in the "zinc-blende-like" structure was also calculated. All structures used in the fit are described in Appendix A. We then constructed an orthogonal two-center TB Hamiltonian using the 4*s* orbital of K, 2*p* orbitals of B, and the 1*s* orbital of H. NRL-TB parameters were obtained by fitting the onsite terms, the two-center Hamiltonian to the electronic eigenvalues and total energies provided by the VASP calculations. The VASP eigenvalues are shifted by a constant energy defined as [11]

$$U_0 = F[n(\mathbf{r})]/N_e, \tag{1}$$

where N_e is the number of electrons in the system and $F[n(\mathbf{r})]$ is the functional of the electron density $n(\mathbf{r})$ that contains the VASP total energy associated with the ion–ion interaction, the Hartree and exchange–correlation energy not included in the eigenvalue sums, and corrections for double counting in the eigenvalue sums. This renders the sum of the shifted eigenvalues equal to the VASP energy.

The on-site TB parameters of an atom i are defined as [11,10]

$$h_{il} = a_l + b_l \rho_i^{\frac{2}{3}} + c_l \rho_i^{\frac{4}{3}} + d_l \rho_i^2, \tag{2}$$

where the coefficients a_l, b_l, c_l, and d_l ($l = s,p$) are the fitting parameters. The atom density ρ_i has the form:

$$\rho_i = \sum_j e^{-\lambda^2 R_{ij}} F(R_{ij}), \tag{3}$$

where the sum is over all atoms j within a range R_c of atom i, λ is a fitting parameter and $F(R_{ij})$ is a cut-off function. In the two-center approximation, the hopping integrals depend only on the angular momentum dependence of the orbitals, $ll'u$, and the distance between the atoms. Here, $ll'u = ss\sigma$ for the K–K, H–H and K–H hopping parameters, $ll'u = (ss\sigma, sp\sigma)$ for K–B and B–H parameters, and $ll'u = (ss\sigma, sp\sigma, pp\sigma, pp\pi)$ for B–B parameters. The hopping parameters for both the Hamiltonian and overlap matrices have the form:

$$H_{ll'u}(R) = (e_{ll'u} + f_{ll'u} R + g_{ll'u} R^2) e^{-q_{ll'u}^2 R} F(R), \tag{4}$$

where R is the separation between the atoms and $e_{ll'u}$, $f_{ll'u}$, $g_{ll'u}$, and $q_{ll'u}$ are the fitting parameters. The overlap parameters which have a form similar to the hopping parameters in Eq. (4) were not used in this work. This form of the TB parameters allows transferability to different crystal structures and atomic configurations.

3. Bulk properties

3.1. Tight-binding parameters

Table 1 lists the lattice parameters of the tetragonal, cubic, and zinc-blende structures obtained in the VASP calculations which formed a database that was used as the input for the TB calculations. We fitted the total energy for a total of 103 structures and volumes in the range shown in Table 1. The energy bands were fitted simultaneously with the total energies but in a narrow range around the equilibrium. Table 2 lists the TB parameters for KBH_4, generated following the NRL-TB method [11].

Fig. 1 shows the variation of the total energy of KBH_4 as a function of volume per unit formula for the cubic and zincblende structures for both VASP and TB. The VASP results for the total energy are reproduced by the TB calculations with a total rms error of 0.022 eV. The calculated total energy versus volume curves are plotted for the tetragonal, cubic, and zinc-blende structures. Each structure has its own minimum of the total energy. For the cubic and zinc-blende structures the energy varies with the lattice constant a or the unit-cell volume with the minimum energy −3.931 eV/atom at the lattice constant of 6.76 Å (cubic) and the minimum energy −3.831 eV/atom at the lattice constant of 8.20 Å (zinc-blende). For the tetragonal structure, the energy also depends on the c/a ratio. The lowest energy is −3.934 eV at $c/a = 1.4$ and $a_{eq.} = 4.78$ Å. The TB equilibrium lattice parameters are almost exactly equal to the VASP values given in Table 1. Note that the equilibrium volumes of the cubic (12.87 $Å^3$/atom) and tetragonal (12.71 $Å^3$/atom) structures are comparable, indicating that the structural transition is not associated with thermal expansion. The difference in cohesive energy between the two structures is 0.003 eV/atom. For the fitting of the energy bands, the associated rms fitting error is 0.160 eV for the three occupied bands and 0.900 eV for the first conduction band in the cubic structure.

3.2. Electronic structure

For the purpose of comparing our TB electronic structure to that given by VASP, we performed a separate fit for only the equilibrium cubic volume that also includes the B *s* orbital. This fit yields a TB band structure in very good agreement with that of VASP, as seen in Figs. 2 and 3. The B *s* (in the energy range from −5 eV to −6 eV) and *p* (from 0 eV to −1.3 eV) occupied states are reproduced as well as the bottom of the conduction band and the energy gap. Fig. 3 shows the total (DOS) and partial (PDOS) density of states, respectively, for cubic KBH_4 from VASP and TB calculations. The valence-band maximum (VBM) consists of the bonding state of B *p* and H *s*, whereas the conduction-band minimum (CBM) consists of predominantly K *s*. Thus K donates one electron to the lattice and becomes K^+. There is, however, strong mixing between B *p* and H *s* states, indicating the B–H bonds are highly covalent. The

Table 1
VASP lattice parameters (c/a and a) used to derive the TB parameters. We also list the VASP equilibrium lattice constant ($a_{eq.}$) which was reproduced almost exactly by the TB fit. The structures are defined in more detail in Appendix A.

Structure	c/a	a (Å)	$a_{eq.}$ (Å)
Cubic		3.70–8.16	6.76
Tetragonal	1.2	4.58–6.38	
Tetragonal	1.3	4.38–6.38	
Tetragonal	1.4	4.18–6.18	4.78
Tetragonal	1.5	4.18–5.98	
Tetragonal	1.6	4.18–5.98	
Tetragonal	1.7	3.98–5.78	
Zinc-blende		7.40–9.00	8.20

Table 2
Tight-binding parameters for KBH_4. On-site energies are generated from the densities of K, B and H atoms: $\rho_K = \sum_K \exp(-\lambda_K^2 R)F(R)$ where $\lambda_K = 1.01006$ a.u.$^{-1/2}$, $\rho_B = \sum_B \exp(-\lambda_B^2 R)F(R)$ where $\lambda_B = 1.22740$ a.u.$^{-1/2}$, and $\rho_H = \sum_H \exp(-\lambda_H^2 R)F(R)$ where $\lambda_H = 1.04039$ a.u.$^{-1/2}$. $F(R)$ is the cutoff function with $R_c = 16.5$ a.u. and $L_c = 0.5$ a.u. All energies are in Rydberg, all distances in a.u.

On-site parameters				
K–K interactions				
$h_l = a_l + b_l\rho_K^{2/3} + c_l\rho_K^{4/3} + d_l\rho_K^2$				
l	a_l	b_l	c_l	d_l
s	1.41085	96.903	−1982.1	21880.0
B–B interactions				
$h_l = a_l + b_l\rho_B^{2/3} + c_l\rho_B^{4/3} + d_l\rho_B^2$				
l	a_l	b_l	c_l	d_l
p	−0.01309	8.1793	17.359	4545.2
H–H interactions				
$h_l = a_l + b_l\rho_H^{2/3} + c_l\rho_H^{4/3} + d_l\rho_H^2$				
l	a_l	b_l	c_l	d_l
s	0.03011	0.42620	−3.8212	9.6246
Hopping terms				
$H_{ll'u}(R) = (e_{ll'u} + f_{ll'u}R + g_{ll'u}R^2)\exp(-q_{ll'u}^2 R)F(R)$				
K–K interactions				
$H_{ll'u}$	$e_{ll'u}$	$f_{ll'u}$	$g_{ll'u}$	$q_{ll'u}$
$H_{ss\sigma}$	−983.31	255.34	−16.211	0.81219
B–B interactions				
$H_{ll'u}$	$e_{ll'u}$	$f_{ll'u}$	$g_{ll'u}$	$q_{ll'u}$
$H_{pp\sigma}$	161.88	12.038	−6.1940	1.0213
$H_{pp\pi}$	14.920	−61.482	9.6289	1.0427
H–H interactions				
$H_{ll'u}$	$e_{ll'u}$	$f_{ll'u}$	$g_{ll'u}$	$q_{ll'u}$
$H_{ss\sigma}$	2.3327	−6.0578	1.9038	1.1324
K–B interactions				
$H_{ll'u}$	$e_{ll'u}$	$f_{ll'u}$	$g_{ll'u}$	$q_{ll'u}$
$H_{sp\sigma}$	−45.346	8.2057	0.46698	0.86962
K–H interactions				
$H_{ll'u}$	$e_{ll'u}$	$f_{ll'u}$	$g_{ll'u}$	$q_{ll'u}$
$H_{sp\sigma}$	75.986	−13.626	−0.67893	1.0965
B–H interactions				
$H_{ll'u}$	$e_{ll'u}$	$f_{ll'u}$	$g_{ll'u}$	$q_{ll'u}$
$H_{sp\sigma}$	1.6293	−0.72728	−0.49906	1.0398

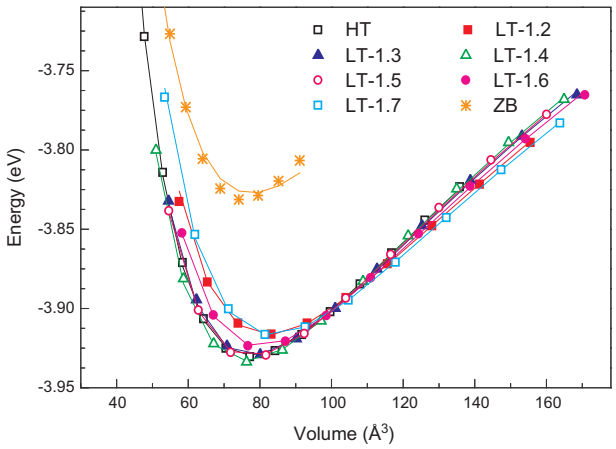

Fig. 1. Total energy versus formula unit volume in tetragonal (LT; $c/a = 1.2, 1.3, 1.4, 1.5, 1.6, 1.7$), cubic (HT), and zinc-blende (ZB) structures: VASP data (symbols) versus TB fit (lines).

compound can be considered as consisting of an ordered arrangement of K^+ and $(BH_4)^-$ units. The calculated VASP band gap of KBH_4 is 6.21 eV. The TB calculations reproduce very well the DOS and PDOS, except for the region about 1.2 eV above the CBM. The

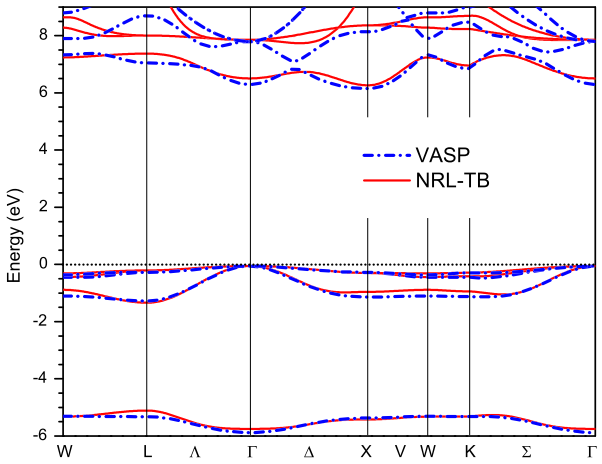

Fig. 2. Band structure of cubic KBH_4. The zero of the energy is set to the highest occupied state.

tetragonal phase gives similar DOS to that of the cubic. We present the TB-VASP comparison of the tetragonal structure in Appendix B as Fig. B.10. For the TB results in the remainder of the article, we did not include the deep B *s* states which are unlikely to affect the states near the Fermi level. However, we added the total energy input for both the cubic and tetragonal structures for 103 volumes as stated in Section 2. The resulting parameters given in Table 2 do not fit the energy bands as well as those used in Figs. 2 and 3, but they reproduce very well the VASP total energy which is the basis of the results described in the next sections. By expanding the physical description to lattice parameters other than the equilibrium ones, we are sacrificing the quality of the TB fit of the energy bands which is not as good as in Fig. 2, but the TB total energies are very good as shown in Fig. 1.

3.3. Elastic constants

The calculations of the elastic constants serve as a sensitive test for the TB parameters because the calculations depend on small differences between the equilibrium energies and the energy with the strain. The strain is applied to the unit cell with the relaxed atomic positions in the cell. We compute the elastic constants of KBH_4 in both the low and high-temperature structures by using finite strains on the equilibrium VASP and TB structures [29,30]. In each case we apply a finite strain to the primitive cell of the crystal, fix the size and shape of the primitive cell, and allow the atoms to relax to the lowest energy structure consistent with the symmetry of the strained unit cell. We have obtained the elastic constants for KBH_4 and compared them with the VASP results. For a given strain matrix $\{e_i\}$, to lowest order the total energy changes from its equilibrium value to

$$E(e_i) = E_0 + \frac{V}{2}\sum_{ij} C_{ij}e_i e_j + O\left[e_i^3\right], \tag{5}$$

where E_0 is the equilibrium energy, V is the volume of undistorted lattice, and the e_i are the strain tensor components, discussed in detail in Refs. [29,30]. The HT cubic lattice has 3 independent elastic moduli. For the volume conserving orthorhombic strain, Eq. (5) is reduced to

$$E(\xi) = E_0 + V(C_{11} - C_{12})\xi^2, \tag{6}$$

where ξ is the strain. The $C_{11} - C_{12}$ modulus is obtained from the slope of $\Delta E = E(\xi) - E_0$ as a function of ξ^2. The C_{44} modulus is calcu-

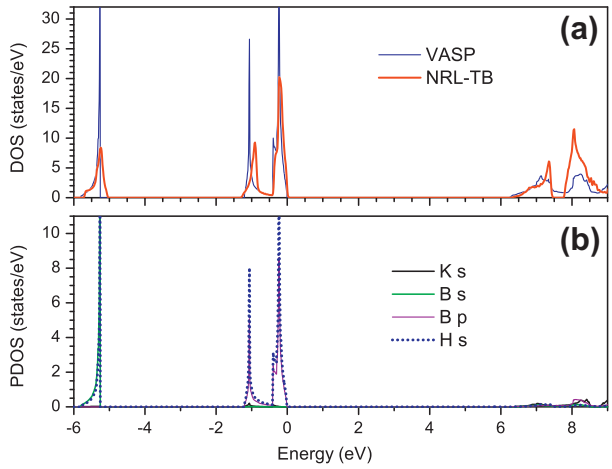

Fig. 3. (a) The total electronic density of states (DOS) and (b) partial density of states (PDOS) of the cubic phase of KBH_4.

lated with a volume conserving orthorhombic strain from the slope of

$$E(\xi) = E_0 + \frac{1}{2} V C_{44} \xi^2. \tag{7}$$

The computed elastic constants are shown in Table 3 for the high-temperature phase and in Table 4 for the low temperature phase. In both cases the elastic constants satisfy the Born stability criteria [31]. The third independent constant is the bulk module

$$B = \frac{C_{11} + 2C_{12}}{3}. \tag{8}$$

The calculated B values are determined from a third-order Birch fit to the energy volume curves [32], and are in agreement with that reported in experiment (16.8 GPa) [18]. Comparing TB and VASP for C_{11}, C_{12} and C_{44} we find a reasonable agreement considering that these elastic constants were not fitted and the material is soft and has small values of C_{ij}.

The LT tetragonal structure has 6 independent elastic constants which are obtained from the slope of $\Delta E = E(\xi) - E_0$ as a function of ξ^2 for six different strains:

$$E(\xi) = E_0 + \begin{cases} V(C_{11} - C_{12})\xi^2 \\ VC_{44}\xi^2 \\ V(C_{11} + C_{12})\xi^2 \\ V(C_{11} + C_{12} + 2C_{13} - 4C_{13})\xi^2 \\ \frac{1}{2}VC_{33}\xi^2 \\ \frac{1}{2}VC_{66}\xi^2 \end{cases}. \tag{9}$$

The bulk modulus is related to these constants by [29,30]

$$B = \frac{(C_{11} + C_{12})C_{33} - 2C_{13}^2}{C_{11} + C_{12} + 2C_{33} - 4C_{13}}. \tag{10}$$

The elastic constants are shown in Table 4.

The TB bulk modulus is in good agreement with VASP as expected from the very good fit of total energy. The TB results are also in good agreement with VASP except for the C_{66} constant where a serious discrepancy occurs.

3.4. Vibrational spectra

Phonon frequencies are obtained from the derivatives of the energy with respect to the displacement of the atoms from their equilibrium lattice positions. In the harmonic approximation, the potential energy as a function of the displacement and the energy variation can be written in the form [33]

$$P_{\text{harm}} = \frac{1}{2} \sum_{\mathbf{R},\mathbf{R}',\alpha,\beta} \mathbf{u}^{\alpha}(\mathbf{R}) \boldsymbol{\eta}^{\alpha\beta}(\mathbf{R} - \mathbf{R}') \mathbf{u}^{\beta}(\mathbf{R}'), \tag{11}$$

where u^{α} is the deviation from equilibrium of atom α on unit cell associated with lattice vector $\mathbf{R}$ and $\boldsymbol{\eta}^{\alpha\beta}(\mathbf{R} - \mathbf{R}')$ is the force constant matrix. The number of independent force constants depends on a symmetry of a phonon mode. We have found the phonon frequencies by the frozen phonon method [33], where a unit cell is commensurate with the wave-vector of the phonon and the displacements of atoms are chosen according to the polarization and the phase of the phonon mode. We used the ISOTROPY package to compute the appropriate unit cells and displacements for each polarization at a given k-point [34].

Figs. 4 and 5 show longitudinal and transverse phonon modes along the Δ line for the cubic structure. The acoustic and optical modes involve the vibrations of all atoms. Fig. 6 shows the transverse Δ_2 optical modes which only involves the hydrogen atoms vibrations. At the Γ point, the wavenumber of a phonon mode is zero and therefore all atoms of the same kind oscillate in phase. The W1 mode involves only the B and H atoms and the W2 mode involves only the K and H atoms. Other modes involve all three kind of atoms: K, B, and H. The frequency depends on the mass of atoms and the force of coupling between them. The GM5, X4, and L2 modes are apparently soft since their frequency is relatively low for light-mass hydrogen atoms. For the Γ-point of tetragonal structure, the phonon modes are listed in Table 5. The Γ_1^+, Γ_3^+, Γ_4^+, Γ_1^-, Γ_2^-, and Γ_4^- modes involve only the hydrogen atoms vibrations. The Γ_3^+ and Γ_2^- appear soft since the frequency is relatively low for a light mass of hydrogen atoms. The TB results are in reasonable agreement with the VASP data, especially since they were not fitted in the determination of our TB parameters.

Table 3
Elastic constants for cubic KBH_4 (in GPa).

	NRL-TB	VASP	Exp.
C_{11}	36.7	30.6	
C_{12}	3.1	5.7	
C_{44}	8.6	7.1	
B	14.3	14.0	16.8 [18]

Table 4
Elastic constants for tetragonal KBH_4 (in GPa).

	NRL-TB	VASP
C_{11}	27.8	23.4
C_{12}	11.3	7.0
C_{33}	35.2	28.0
C_{13}	2.8	1.6
C_{44}	12.4	12.5
C_{66}	15.5	6.4
B	13.8	10.6

3.5. Mean-squared displacement

Using the TB parameters reported in Table 2, we performed molecular dynamics (MD) simulations [35] for a supercell of the cubic KBH_4. The supercell of 384 atoms is obtained by repeating the primitive cell 4 times along each of the primitive lattice directions. The simulations were performed for 1000 steps with a time step of 0.5 fs at a temperature T. Initially, the atoms are placed on the lattice with random velocities with a Boltzmann distribution function for a temperature of $2T$. Very quickly, in approximately

60 fs (300 steps), the atomic motion slows down to the average velocities and displacements corresponding to the equilibrium at T.

For the cubic KBH_4 phase, we have determined the atomic mean-squared displacement of the K, B and H atoms for various temperatures between 50 K and 170 K using the atomic positions recorded in the process of the MD simulation; see Fig. 7. First, we recorded the instantaneous positions $\mathbf{r}_j(n)$ of 128 atoms j at each simulation step n for the substantially large number of steps N in the range from $n = n_0$ to $n = n_0 + N$. Next, we calculated the statistical mean-squared displacement by averaging the deviation of atomic positions squared over the snapshots recorded: $u_j^2 = \sqrt{\sum_{n=n_0}^{n_0+N}(\mathbf{r}_j(n) - \mathbf{r}_j(n_0))^2/N}$. Finally, we averaged the mean squared displacements for each atom over all atoms of the same kind: hydrogen $u_H^2 = \sum_{j\in H} u_j^2/256$, potassium $u_K^2 = \sum_{j\in K} u_j^2/64$, or boron $u_B^2 = \sum_{j\in B} u_j^2/64$. In the range of relatively low temperatures, the mean-squared displacement changes linearly with the temperature. In Fig. 7 it is noted that the displacement of B atoms is smaller than that of K and H, although B is lighter than K. This is probably due to the strong B–H bonding and B and H should be considered in terms of BH_4 units, not as individual atoms.

4. Hydrogen vacancies

We studied the structure and energetics of native defects in the tetragonal and cubic KBH_4 phases using both VASP and NRL-TB. Our purpose is not to carry out a comprehensive study of the defects in the compound, but to focus only on the hydrogen vacancies and see if the NRL-TB method can reproduce the structure and energetics obtained in VASP calculations. For these calculations we used various supercell sizes that contain up to 4374 atoms/cell, and 4 **k**-points. The creation of V_H^- involves removing a proton (H^+) from the KBH_4 supercell, and this results in a BH_3 unit. V_H^0 is created by removing one H atom from the system, and this leads to formation of a trigonal planar BH_3 unit. V_H^+, created by removing one H atom and an extra electron, results in a BH_3 unit that is similar to that of V_H^0. The structure of V_H^+ in KBH_4 is thus different from that in $LiBH_4$ where V_H^+ leads to the formation of a BH_3–H–BH_3 complex (two BH_4 units sharing a common H ion) [9]. The reason is that the B–B distance (4.8 Å) in KBH_4 is larger than that (4.3 Å) in $LiBH_4$, making the BH_3–H–BH_3 configuration energetically less favorable. The defect structures are found to be similar in both the cubic and tetragonal phases as well as in both VASP and TB calculations.

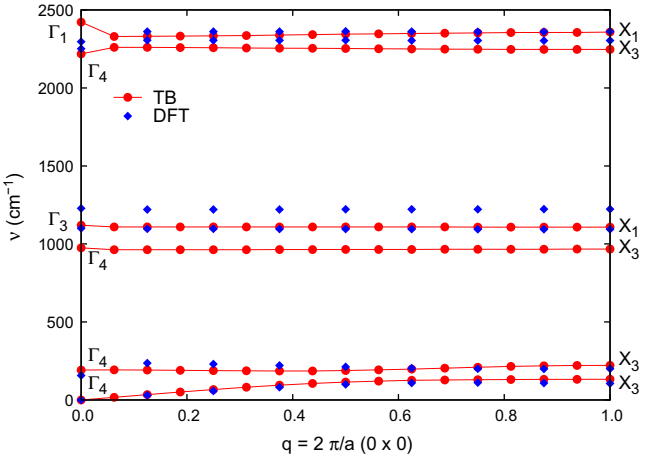

Fig. 4. Δ_1 phonons for the cubic KBH_4.

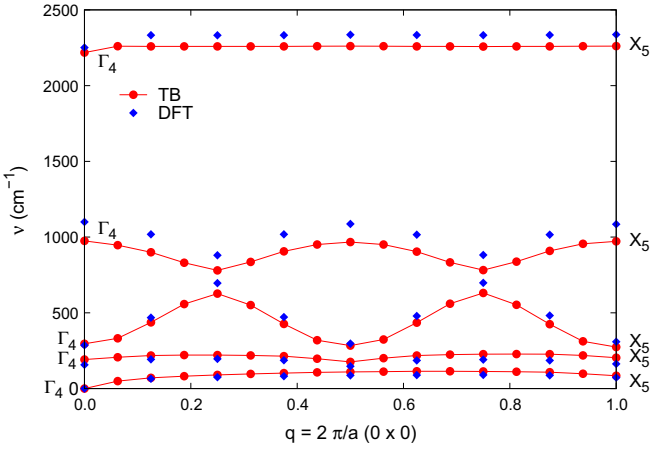

Fig. 5. Δ_{34} phonons for the cubic KBH_4.

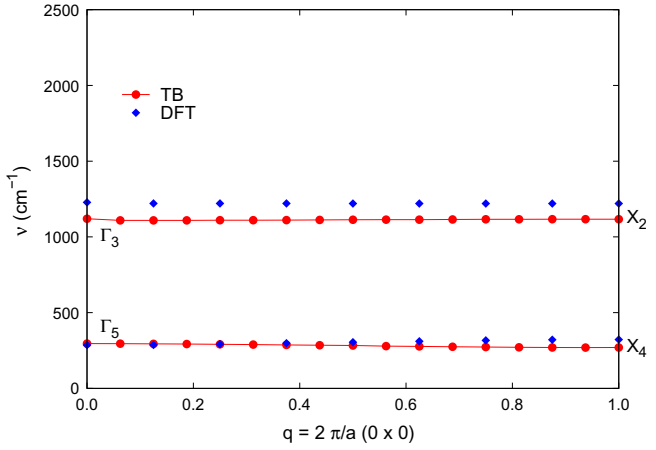

Fig. 6. Δ_2 phonons for the cubic KBH_4.

Table 5
Phonon frequency (in cm^{-1}) for tetragonal KBH_4 at the Γ point.

	NRL-TB	VASP		NRL-TB	VASP
Γ_1^+	723	1167	Γ_1^-	690	1216
Γ_1^+	2080	2201	Γ_2^-	193	294
Γ_2^+	137	107	Γ_3^-	0	0
Γ_2^+	194	190	Γ_3^-	168	160
Γ_2^+	766	1088	Γ_3^-	765	1084
Γ_2^+	2467	2370	Γ_3^-	2462	2349
Γ_3^+	211	324	Γ_4^-	697	1215
Γ_4^+	708	1216	Γ_4^-	2264	2318
Γ_5^+	91	71	Γ_5^-	0	0
Γ_5^+	161	166	Γ_5^-	167	161
Γ_5^+	210	307	Γ_5^-	175	285
Γ_5^+	779	1086	Γ_5^-	757	1082
Γ_5^+	2468	2350	Γ_5^-	2463	2338

We employ defect formation energies to characterize different defects. Defects with low formation energies will easily form and occur in high concentrations. The formation energy of a hydrogen vacancy in charge state q (hereafter denoted as V_H^q) is defined as [36]

$$E^f = E_{tot}(V_H^q) - E_{tot}(\text{bulk}) + \mu_H + q(E_V + \mu_e), \quad (12)$$

where $E_{tot}(V_H^q)$ and $E_{tot}(\text{bulk})$ are, respectively, the total energies of a supercell containing the vacancy V_H^q, and of a supercell of the

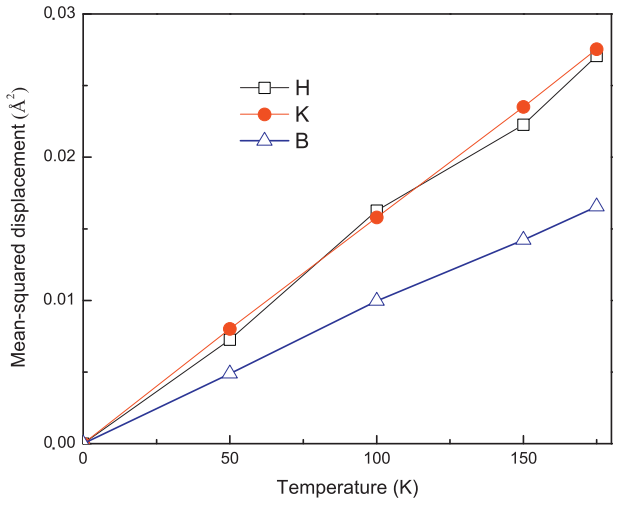

Fig. 7. Mean-squared displacement for K, B, and H atoms.

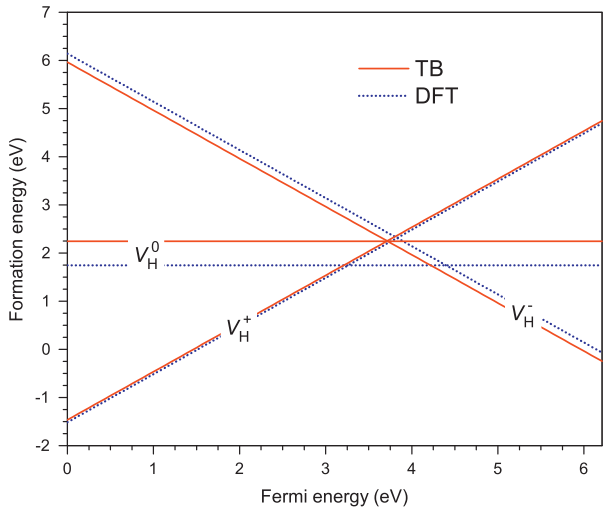

Fig. 8. Calculated formation energies of hydrogen vacancies in the cubic KBH_4 phase, plotted as a function of Fermi energy with respect to the VBM. The slope in the formation energy plots indicates the charge state.

perfect bulk material. μ_e is the electron chemical potential, i.e., the Fermi level, referenced to the VBM in the bulk (E_V). μ_H is the hydrogen chemical potential (and is referenced to H_2 molecules at 0 K), which is a variable and can be chosen to represent experimental conditions. In the following presentation, we set $\mu_H = -0.59$ eV which corresponds to assuming thermal equilibrium with H_2 gas at 1 bar and 585 °C [37], the decomposition temperature and also the melting temperature of KBH_4 [2].

Fig. 8 shows the calculated formation energies of hydrogen vacancies in various charge states ($q = 0, \pm 1$) in the cubic KBH_4 phase. The VASP and TB results were obtained from calculations using a 192-atom supercell. Note that with the set of TB parameters given in Table II, the calculated TB band gap is 5.10 eV, whereas the VASP band gap is 6.21 eV. We adjust the band gap difference by shifting the conduction band in the TB calculations up in the energy by 1.11 eV. The formation energy of V_H^- is therefore shifted by the same amount, assuming that the defect state associated with V_H^- is coupled to the conduction band. Our results show that there is excellent agreement between TB and VASP calculations in the case of V_H^+ (the formation energy difference is about 0.1 eV). The difference is larger for V_H^0 (~0.5 eV) and for V_H^- (~0.2 eV, after adjusting for the band gap discrepancy). The TB *vis-à-vis* VASP results for the hydrogen vacancy formation energies clearly reflect the degree to which the TB calculations can reproduce the VASP electronic structure. With the set of TB parameters given in Table II, the valence band is well reproduced by the TB calculations, while the conduction band is not. This is the reason why there is good agreement in the case of V_H^+, since the defect state associated with V_H^+ is strongly coupled to the valence band, whereas the agreement is poor in the case of V_H^- because its defect state is strongly coupled to the conduction band. Note that the calculated formation energies of the vacancies in the tetragonal and cubic phases are almost the same (the energy difference is within 30 meV in VASP calculations).

Fig. 9 shows the formation energy of the positively charged hydrogen vacancy V_H^+ at the VBM (i.e., μ_e=0 eV) as a function of the number of atoms in the supercell, obtained in TB and VASP calculations. We find that the formation energy value (at the VBM) reaches −1.41 eV in supercells with more than 2000 atoms where it becomes well converged in the TB. It is clear that the VASP results up to a 750-atom supercell size have not converged. It is not computationally practical to continue the VASP calculations to larger supercells. This brings an important advantage of our TB approach in terms of computational efficiency.

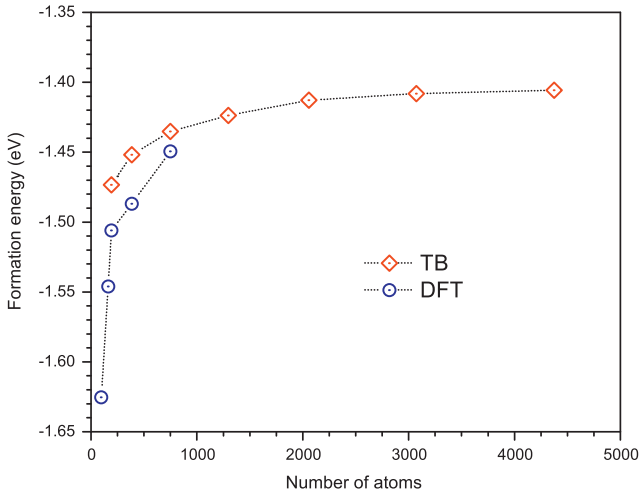

Fig. 9. The formation energy of V_H^+ at the VBM as a function of the supercell size.

5. Summary

We have used the NRL-TB method to perform both static and dynamic calculations of various properties of KBH_4. This work capitalizes on the fact that the NRL-TB method substantially reduces the computational cost in comparison with first-principles methods. Overall, our TB results for the structural, electronic, elastic, and vibrational properties of KBH_4 show good agreement with the fitted VASP results. For quantities that were not fitted such as formation of hydrogen vacancies, we find reasonable agreement with independent VASP results. In addition, the present TB Hamiltonian performs significantly faster than VASP for cases such as the calculation of mean-squared displacements where large supercells are needed. In the calculations of hydrogen vacancies, we performed tests of the supercell size that the TB can handle. We found that supercells with more than 4000 atoms can be done with modest computational cost, while VASP calculations for such a large supercell are not practical. In the hydrogen vacancy application presented in this paper, convergence for supercell size is achieved at about 2000 atoms.

Table A.6
The equilibrium low temperature structure of KBH_4, as determined by Renaudin et al. [14]. The structural parameterization given here is the equilibrium value from our VASP simulation.

Space group	$P4_2/nmc$ (#137)		
Lattice constants			
(a,b,c) (Å)	4.714	4.717	6.617
(α,β,γ)	90	90	90
Wyckoff positions			
K (4*b*)	0.250	0.750	0.750
B (4*a*)	0.250	0.750	0.250
H (8*g*)	0.250	0.537	0.357

Table A.7
The approximate high-temperature structure of KBH_4, used in our VASP and TB simulations.

Space group	$F\bar{4}3$ m (#216)		
Lattice constants			
(a,b,c) (Å)	6.76	6.76	6.76
(α,β,γ)	90	90	90
Wyckoff positions			
K (4*a*)	0.000	0.000	0.000
B (4*b*)	0.500	0.500	0.500
H (16*e*)	0.395	0.395	0.605

Table A.8
The ficticious "zinc-blende" structure of KBH_4, used in our VASP and TB simulations.

Space group	$F\bar{4}3$ m (#216)		
Lattice constants			
(a,b,c) (Å)	8.60	8.60	8.60
(α,β,γ)	90	90	90
Wyckoff positions			
K (4*d*)	0.250	0.250	0.250
B (4*b*)	0.500	0.750	0.500
H (16*e*)	0.418	0.418	0.582

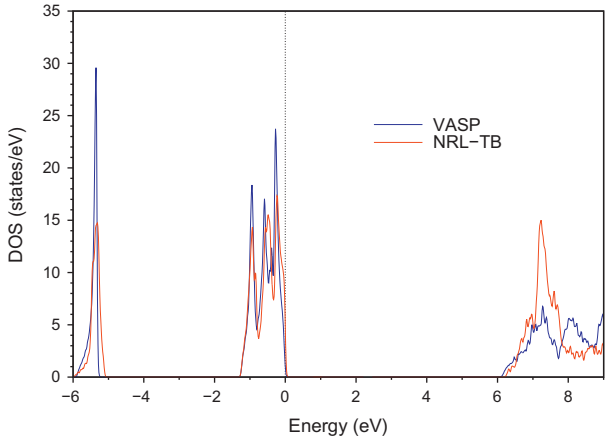

Fig. B.10. Total electronic density of states comparing TB to VASP for the tetragonal phase.

Acknowledgments

We thank N. Bernstein for helpful discussions and H. Stokes for the use of the ISOTROPY package. This work was partially supported by the U.S. Department of Energy (Grant No. DE-FG02-07ER46425) and made use of NERSC resources supported by the DOE Office of Science (Contract No. DE-AC02-05CH11231). K.H. was supported by the U.S. Naval Research Laboratory (Grant No. NRL-N00173-08-G001) and by the Center for Computationally Assisted Science and Technology (CCAST) at North Dakota State University. N.K. was supported by NSF (Grant No. DMR-1205734). M.M. was supported by the U.S. Office of Naval Research. Some VASP calculations were performed at the U.S. Department of Defense ERDC and AFRL High-Performance Computing Resource Centers.

Appendix A. Description of the crystal structures

In this Appendix we briefly describe the crystal structures used in the TB fit. The low temperature ("tetragonal" in Table 1) structure is that described by Renaudin et al. [14] The VASP equilibrium structure is given in Table A.6. In this structure the hydrogen atoms form a tetrahedron around each boron atom, with every hydrogen positioned along a line between the boron atom and a nearest-neighbor potassium atom. All of the hydrogen tetrahedra in a given (100) plane are oriented in the same direction, and alternate planes have the opposite orientation, consistent with the $P4_2/nmc$ space group.

The high-temperature ("cubic" in Table 1) structure described by Renaudin et al. is similar to the low-temperature structure, but now the hydrogen tetrahedra are randomly ordered. The structure is described as a fcc lattice, space group $Fm\bar{3}m$ (#225), but the hydrogen tetrahedra only partially fill the (32*f*) Wyckoff sites. We cannot model a partially filled site either with VASP or NRL-TB, so for our calculations we required all of the hydrogen tetrahedra to be oriented in the same direction, while keeping the fcc lattice. This reduces the symmetry from $Fm\bar{3}m$ to $F\bar{4}3$ m (#216), with the atomic positions described in Table A.7. This approximate structure can be thought of as a decorated sodium-chloride structure, where the potassium ions are on the sodium sites and the BH_4 tetrahedra are on the chlorine sites. This suggests an alternative structure would have a cubic "zinc-blende" orientation. We constructed such a structure, as described in Table A.8, and used it in the fit over the range of lattice constants listed in Table 1.

Appendix B. Density of states for tetragonal phase

Fig. B.10 presents results for the calculations of the total electronic density of states for the low-temperature tetragonal phase of KBH_4. The agreement between TB and VASP is very good.

References

[1] U. Eberle, M. Felderhoff, F. Schüth, Angew. Chem. Int. Ed. 48 (2009) 6608.
[2] S.-I. Orimo, Y. Nakamori, J.R. Eliseo, A. Züttel, C.M. Jensen, Chem. Rev. 107 (2007) 4111.
[3] A. Peles, C.G. Van de Walle, Phys. Rev. B 76 (2007) 214101.
[4] K. Hoang, C.G. Van de Walle, Phys. Rev. B 80 (2009) 214109.
[5] G.B. Wilson-Short, A. Janotti, K. Hoang, A. Peles, C.G. Van de Walle, Phys. Rev. B 80 (2009) 224102.
[6] K. Hoang, A. Janotti, C.G. Van de Walle, Angew. Chem. Int. Ed. 50 (2011) 10170.
[7] K. Hoang, A. Janotti, C.G. Van de Walle, Phys. Rev. B 85 (2012) 064115.
[8] K. Hoang, A. Janotti, C.G. Van de Walle, Phys. Chem. Chem. Phys. 14 (2012) 2840.
[9] K. Hoang, C.G. Van de Walle, Int. J. Hydrogen Energy 37 (2012) 5825.
[10] R.E. Cohen, M.J. Mehl, D.A. Papaconstantopoulos, Phys. Rev. B 50 (1994) 14694.
[11] M.J. Mehl, D.A. Papaconstantopoulos, Phys. Rev. B 54 (1996) 4519.
[12] A. Shabaev, D.A. Papaconstantopoulos, Phys. Rev. B 79 (2009) 064107.
[13] A. Shabaev, D.A. Papaconstantopoulos, M.J. Mehl, N. Bernstein, Phys. Rev. B 81 (2010) 184103.
[14] G. Renaudin, S. Gomes, H. Hagemann, L. Keller, K. Yvon, J. Alloys Comp. 375 (2004) 98.
[15] M.E. Arroyo y De Dompablo, G. Ceder, J. Alloys Comp. 364 (2004) 6.
[16] P. Vajeeston, P. Ravindran, A. Kjekshus, J. Alloys Comp. 387 (2005) 97.
[17] K.C. Kim, D.S. Sholl, J. Phys. Chem. C 114 (2010) 678.
[18] R.C. Kumar, E. Kim, A.L. Cornelius, J. Phys. Chem. C 112 (2008) 8452.
[19] X.-D. Zhang, Z.-F. Hou, Z.-Y. Jiang, Y-Q. Hou, Physica B 406 (2011) 2196.
[20] H. Hagemann, S. Gomes, G. Renaudin, K. Yvon, J. Alloys Comp. 363 (2004) 126.

[21] J.P. Perdew, K. Burke, M. Ernzerhof, Phys. Rev. Lett. 77 (1996) 3865.
[22] P.E. Blöchl, Phys. Rev. B 50 (1994) 17953.
[23] G. Kresse, J. Hafner, Phys. Rev. B 59 (1999) 1758.
[24] G. Kresse, J. Hafner, Phys. Rev. B 47 (1993) 558.
[25] G. Kresse, J. Hafner, Phys. Rev. B 49 (1994) 14251.
[26] G. Kresse, J. Furthmüller, Comput. Mater. Sci. 6 (1996) 15.
[27] G. Kresse, J. Furthmüller, Phys. Rev. B 54 (1996) 11169.
[28] H.J. Monkhorst, J.D. Pack, Phys. Rev. B 13 (1976) 5188.
[29] M.J. Mehl, J.E. Osburn, D.A. Papaconstantopoulos, B.M. Klein, Phys. Rev. B 41 (1990) 10311.
[30] M.J. Mehl, B.M. Klein, D.A. Papaconstantopoulos, in: J.H. Westbrook, R.L. Fleischer (Eds.), Intermetallic Compounds: Principles and Applications, vol. 1, Wiley, London, 1994.
[31] M. Born, K. Huang, Dynamical Theory of Crystal Lattices, Oxford Press, Oxford, 1966.
[32] F. Birch, J. Geophys. Res. 83 (1978) 1257.
[33] S.W. Wei, M.Y. Chou, Phys. Rev. Lett. 69 (1992) 2799.
[34] H.T. Stokes, D.M. Hatch, B.J. Campbell, ISOTROPY (2007). <http://www.stokes.byu.eduisotropy.html>.
[35] F. Kirchhoff, M.J. Mehl, N.I. Papanicolaou, D.A. Papaconstantopoulos, F.S. Khan, Phys. Rev. B 63 (2001) 195101.
[36] C.G. Van de Walle, J. Neugebauer, J. Appl. Phys. 95 (2004) 3851.
[37] H. Hemmes, A. Driessen, R. Griessen, J. Phys. C: Solid State Phys. 19 (1986) 3571.